Check for updates

Zwitterionic MRI contrast agents with enhanced relaxivity, stability and reduced renal retention

Lennart F. V. Spickschen,[a] Verena R. Schulze,[b] Michael G. Kaul,[c] Darius Ludolfs,[a] Marie Oest,[d] Daniel L. J. Thorek,[e] Neus Feliu,[b] Markus Fischer, [ID][d] John V. Frangioni[f] and Wolfgang Maison [ID] *[a]

Concerns over *in vivo* Gd(III) retention have recently prompted the development of Gd(III)-based contrast agents (GBCAs) with high-relaxivity and stability. This work describes the synthesis of a novel modular and enantiomerically pure chelator, (*R,R,R*)-Bn$_3$-PCTAZA **8** allowing modification *via* Cu(I)-catalyzed alkyne-azide cycloaddition (CuAAC). Two zwitterionic GBCAs, Gd-SB$_3$-PCTA **11a** and Gd-NOx$_3$-PCTA **12a**, were prepared by CuAAC and analysed for important physicochemical properties and complex stability. Both zwitterionic complexes have improved kinetic inertness compared to the clinically relevant GBCA gadopiclenol **3**. In addition, Gd-SB$_3$-PCTA **11a** revealed an 18% increase in relaxivity (r_1) compared to gadopiclenol **3**. Gd-NOx$_3$-PCTA **12a**, has a slightly lower relaxivity but the highest kinetic stability among all complexes tested. Both agents maintain high relaxivity at clinically relevant magnetic field strengths (1.4 T and 7 T) and have high inertness under transmetallation conditions, acidic conditions and in human serum. These favourable characteristics are due to enhanced second-sphere hydration of the kosmotropic periphery of the complexes. Gd-SB$_3$-PCTA **11a** revealed a significantly reduced retention in mice kidneys compared to gadopiclenol **3**. The zwitterionic GBCAs Gd-SB$_3$-PCTA **11a** and Gd-NOx$_3$-PCTA **12a** are thus promising candidates for the development of next-generation contrast agents for magnetic resonance imaging (MRI).

Introduction

Gd(III)-based contrast agents (GBCAs) are widely used for magnetic resonance imaging (MRI). However, concerns about their long-term safety have led to the withdrawal of some derivatives and are a motivation for the development of safer contrast agents.[1] GBCA administration has been linked to nephrogenic systemic fibrosis (NSF) in patients with impaired renal function.[1–3] In addition, recent studies have demonstrated that repeated administration of certain GBCAs results in the accumulation of Gd(III) even in patients with normal renal function and may result in unwanted physiological effects.[4–8] The accumulation of free Gd(III) is a consequence of Gd(III)-release from GBCAs and regulatory authorities have thus restricted the use of GBCAs containing acyclic Gd(III) chelators, which form Gd(III)-complexes with limited *in vivo* stability.[9,10] However, even GBCAs containing macrocyclic chelators lead to accumulation of Gd(III) *in vivo*. This Gd(III)-retention is not due to a release of free Gd(III) from the complexes but rather a consequence of an unwanted accumulation of the complete GBCAs in certain tissues (particularly the kidney).[11,12] The accumulation of GBCAs is notable considering the efficient clearance of these compounds from the body. To reduce these risks there is an ongoing search for new GBCAs with higher complex stability, improved clearance, and higher relaxivity.[13,14] High T_1-relaxivity GBCAs at equal concentrations induce greater relaxation rate changes, enhancing T_1-weighted image contrast more effectively and allowing for lower dosing than agents with lower relaxivity.[15]

A promising strategy to increase relaxivity is to increase the inner-sphere hydration number q of the Gd(III) complex. However, the increase of inner sphere water molecules is typically associated with a loss of kinetic and thermodynamic stability of the complex. Most stable Gd(III)-complexes of macrocyclic chelators have therefore a hydration number of $q \sim 1$.

A notable exception is gadopiclenol **3** (Fig. 1), a highly stable Gd-complex with a hydration number $q = 2$.[16–18] Gadopiclenol is a chiral Gd(III) complex based on the macrocyclic chelator

[a] *Department of Chemistry, Institute of Pharmacy, University of Hamburg, Bundesstrasse 45, 20146 Hamburg, Germany. E-mail: wolfgang.maison@uni-hamburg.de*

[b] *Fraunhofer Institute for Applied Polymer Research IAP, Center for Applied Nanotechnology CAN, Grindelallee 117, 20146 Hamburg, Germany*

[c] *Department of Diagnostic and Interventional Radiology and Nuclear Medicine, Center of Radiology and Endoscopy, University Medical Center Hamburg-Eppendorf, 20246 Hamburg, Germany*

[d] *Hamburg School of Food Science, Institute of Food Chemistry, University of Hamburg, Grindelallee 117, 20146 Hamburg, Germany*

[e] *Department of Radiology, Washington University, School of Medicine, Drummond Hall, 3691 Rutger St., St. Louis, MO 63110, USA*

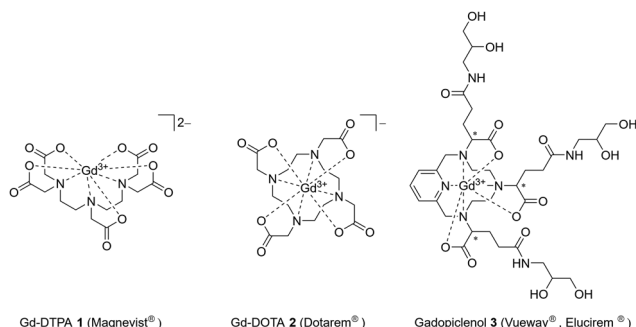[f] *Curadel Pharma, 28120 Hunters Ridge Blvd, Suites 6-7, Bonita Springs, FL 34135, USA*

Fig. 1 Structures of three clinically used GBCAs: Gd-DTPA **1** (Magnevist®), Gd-DOTA **2** (Dotarem®) and gadopiclenol **3** (Vueway®, Elucirem®).

PCTA and has a relaxivity more than twice as high as the relaxivity of other GBCAs in clinical use.[19] PCTA derivatives are thus a promising platform for the development of next-generation GBCAs combining high relaxivity with stability.[19]

The introduction of zwitterionic groups ("zwitterionization"), such as sulfobetaines or amine N-oxides is an additional strategy to enhance the longitudinal relaxivity of GBCAs. The decoration of Gd-DOTA with zwitterions increased its longitudinal relaxivity significantly.[20,21] This enhancement was attributed to two main factors: first, the presence of zwitterions accelerated the exchange rate of inner-sphere water molecules by reducing their mean residence time. Second, the kosmotropic properties of these groups increased the hydrodynamic diameter of the complex and promoted the formation of an extended hydration layer.[22] Together, these effects caused a 2- to 2.5-fold increase in relaxivity compared to non-zwitterionic analogues.[20,21] In addition, zwitterionization of drugs can lead to favourable pharmacokinetic

properties because it leads to efficient renal clearance and decreases unwanted tissue retention.[23,24]

This study describes the synthesis and physicochemical evaluation of two zwitterionic GBCAs (Gd-SB$_3$-PCTA **11a** and Gd-NOx$_3$-PCTA **12a**). Both have been synthesized from the chiral azide-functionalized PCTA derivative (R,R,R)-Bn$_3$-PCTAZA **8**. The approach addresses the following research questions: (1) Can zwitterionic groups enhance the relaxivity of Gd-PCTA complexes? (2) Are zwitterionic Gd-PCTA complexes thermodynamically and kinetically stable? (3) What is the hydration number of the zwitterionic complexes? (4) What is the influence of zwitterionic groups on the in vivo Gd-retention after repeated dosage?

Results and discussion

Synthesis of zwitterionic chelators and corresponding complexes

The new clickable chelator (R,R,R)-Bn$_3$-PCTAZA **8** (Scheme 1) was prepared via alkylation of 3,6,9-triaza-1(2,6)-3,6,9,15-tetraazabicyclo[9.3.1]pentadeca-1(15),11,13-triene (**7**, pyclen) with triflate (S)-**6** using a modified procedure for the alkylation of cyclen.[25] Triflate (S)-**6** was available in enantiomerically pure form from alcohol (S)-**5**, which was prepared from L-malic acid in five steps.[25,26] Alkylation of pyclen **7** with triflate (S)-**6** gave the azide-functionalized chelator (R,R,R)-Bn$_3$-PCTAZA **8** in high yield. Notably, the yield of the alkylation step increased substantially when the triflate was added at 0 °C instead of room temperature. (R,R,R)-Bn$_3$-PCTAZA **8** was prepared in gram quantities with this procedure. The alkylation of pyclen with triflate **8** gives stereoisomerically pure (R,R,R)-Bn$_3$-PCTAZA **8**
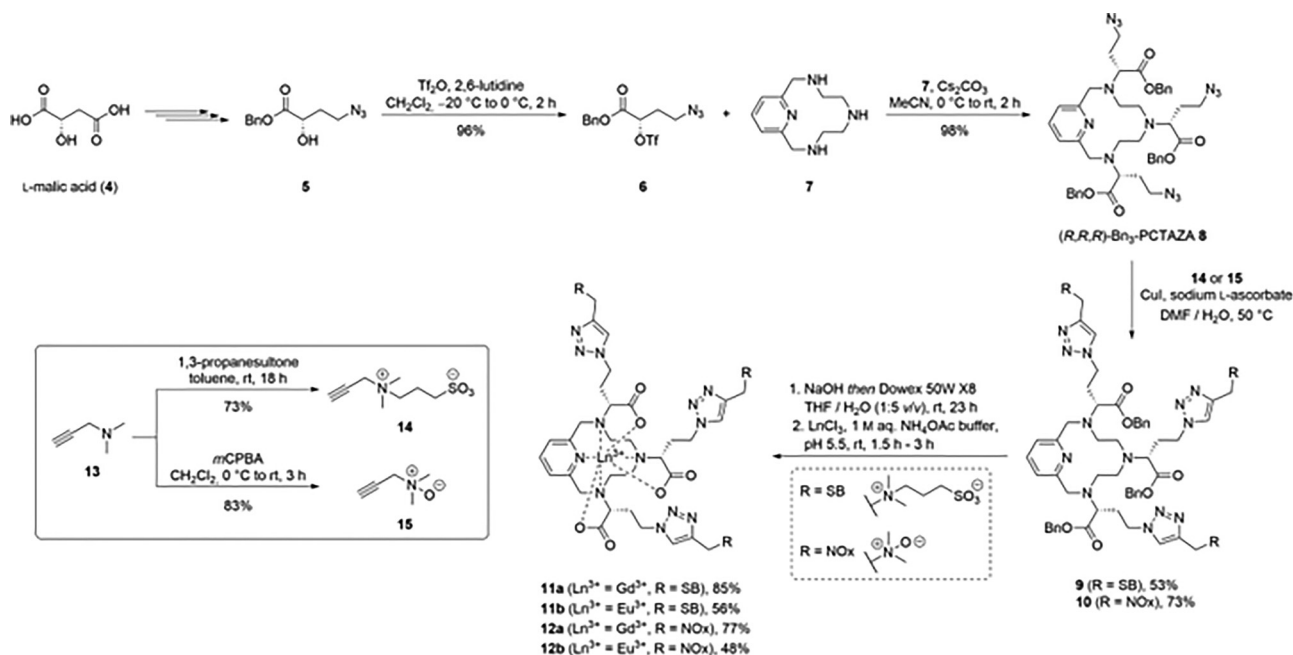
Scheme 1 Synthesis of the azide-functionalised chelator (R,R,R)-Bn$_3$-PCTAZA **8** and its subsequent conversion into the zwitterionic chelators **9** and **10**, followed by complexation with Gd(III) and Eu(III).

according to NMR and HPLC. This indicates a pure S_N2-mechanism and parallels our observations with the alkylation of cyclen *via* the same reaction.[27] The preparation of (*R,R,R*)-Bn$_3$-PCTAZA **8** *via* alkylation with (*S*)-triflate **6** is thus advantageous compared to other approaches, which lead to mixtures of stereoisomers and thus cumbersome separations and low overall yields of the final pure stereoisomers.[19] The modification of (*R,R,R*)-Bn$_3$-PCTAZA **8** *via* CuAAC (click-chemistry) was performed according to an established protocol for the preparation of zwitterionic DOTA-derivatives with the alkynes **14** and **15**.[20,21] Particular attention should be paid to the amount of alkyne used in the CuAAC reactions. In the case of the sulfobetaine alkyne **14**, 3.30 equiv. were sufficient to achieve complete conversion to Bn$_3$-SB$_3$-PCTA **9**. The moderate isolated yield of 53% is a consequence of the high polarity of the compound, which led to problems in the chromatographic separation of Bn$_3$-SB$_3$-PCTA **9** from salts. HPLC-MS analysis of the crude product indicated quantitative formation of **9** with no significant formation of side products. In contrast, a large excess (18.0 eq.) of alkyne *N*-oxide **15**, was required to achieve complete and clean conversion to Bn$_3$-NOx$_3$-PCTA **10**. The reason is a competing copper-catalysed *N-O*-deoxygenation of alkyne **15** or the click-product **10**.[28] Using lower amounts of alkyne *N*-oxide **15** or extending the reaction time for the CuAAC beyond 2 h, consistently led to complex mixtures containing deoxygenated by-products together with the desired product Bn$_3$-NOx$_3$-PCTA **10**. A reaction time of approximately 1 h was optimal and gave reproducible and clean conversions to **10**.

The benzyl esters of Bn$_3$-SB$_3$-PCTA **9** and Bn$_3$-NOx$_3$-PCTA **10** were hydrolysed under alkaline conditions using NaOH in a THF/H$_2$O mixture. The reaction mixture was neutralised by treatment with an acidic ion-exchange resin, which was subsequently removed *via* filtration, affording the zwitterionic chelators SB$_3$-PCTA and NOx$_3$-PCTA in almost quantitative yields. Complexation was performed with GdCl$_3$ or EuCl$_3$ at room temperature in aqueous 1 M NH$_4$OAc buffer (pH 5.5). The resulting complexes Gd-SB$_3$-PCTA **11a** and Gd-NOx$_3$-PCTA **12a** were obtained in good yields over two steps. The complexation was monitored by HPLC-MS, and notably, no free ligand was detected after 10 minutes, indicating a rapid and efficient complexation of both cations.

Eu(III) complexes allow the determination of the inner-sphere hydration number q *via* luminescence lifetime measurements.[29] Complexes Eu-SB$_3$-PCTA **11b** and Eu-NOx$_3$-PCTA **12b** are thus important model compounds for physicochemical characterisation.

It is notable that all zwitterionic complexes had a water solubility greater than 0.5 M. The $\log D_{7.4}$ values of the zwitterionic GBCAs were assessed using a standard shake flask-method (*n*-octanol/PBS). However, quantification was not feasible, as extraction into the *n*-octanol phase was below the HPLC-DAD detection limit. A $\log D$ of -4.2 has been reported for gadopiclenol **3**, but the authors noted that the method used reaches its practical limit for compounds of such high hydrophilicity.[16] Gd-SB$_3$-PCTA **11a** and Gd-NOx$_3$-PCTA **11b** are even more polar than gadopiclenol **3**. We measured the RP-

HPLC retention times with identical separation parameters: gadopiclenol **3** eluted at 9.8 min, whereas Gd-SB$_3$-PCTA **11a** and Gd-NOx$_3$-PCTA **11b** eluted at 9.3 min and 2.3 min respectively. This trend indicates that both zwitterionic derivatives are significantly more hydrophilic than gadopiclenol.

Kinetic and thermodynamic stability of zwitterionic Gd(III) complexes

Kinetic inertness is a key determinant of the *in vivo* stability of GBCAs, as it governs the resistance of the complex to decomplexation processes under physiological conditions. Dissociation of macrocyclic lanthanide complexes occurs *via* protonation of the complex, leading to the formation of a diprotonated intermediate, which then undergoes loss of Gd(III). This process of decomplexation can be monitored by spectrophotometric quantification of free Gd(III) using complexometric titration with Arsenazo III.[16,30,31] The stability of Gd-SB$_3$-PCTA **11a** and Gd-NOx$_3$-PCTA **12a** was assessed in aqueous solution at pH 1.2 and compared to that of gadopiclenol **3** as well as Gd-DOTA **2** (gadoteric acid) under identical conditions.

As previously reported by Robic *et al.*, gadopiclenol **3** is significantly more stable than Gd-DOTA **2** and far more stable than the more labile GBCAs gadodiamide and gadobutrol.[16] This stability trend was confirmed for gadopiclenol **3** and Gd-DOTA **2** in our experiments as depicted in Fig. 2. Notably, the zwitterionic complexes Gd-SB$_3$-PCTA **11a** and Gd-NOx$_3$-PCTA **12a** are more stable under acidic conditions than gadopiclenol **3**. After 21 days, gadopiclenol **3** was completely dissociated, while Gd-SB$_3$-PCTA **11a** released only 62% and Gd-NOx$_3$-PCTA **12a** just 16% of its Gd(III) content (Fig. 2).

The dissociation data of the Gd(III) complexes were evaluated under the assumption that both zwitterionic and non-zwitterionic complexes follow pseudo-first order dissociation kinetics. Linearisation according to the equation $\ln(A_t/A_0) = -k_{\text{obs}} \cdot t$ followed by linear regression, gave the dissociation rate constants k_{obs}. The parameter A_t denotes the concentration of dissociated complex at time t and A_0 the initial concentration of the complex.

Comparison of the observed dissociation rate constants and the total amount of Gd(III) released after 21 days revealed significant differences in the kinetic stability of the complexes. The most stable compound, Gd-NOx$_3$-PCTA **12a** had a dissociation rate that was more than 36-fold lower than that of Gd-DOTA **2** and 15-fold lower than that of gadopiclenol **3**. Notably, Gd-NOx$_3$-PCTA **12a** also dissociated 5.5 times more slowly than the sulfobetaine-analogue Gd-SB$_3$-PCTA **11a**, highlighting a substantial difference in complex stability among zwitterionic complexes. However, both new complexes Gd-SB$_3$-PCTA **11a** and Gd-NOx$_3$-PCTA **12a** are exceptionally stable under acidic conditions with dissociation rates 3 or 15 times lower respectively than that of gadopiclenol **3**.

In summary, these findings reveal a stabilising effect of zwitterionic modifications on the kinetic inertness of the complexes. They suggest that the zwitterionic hydration shell may contribute to an intramolecular pH buffering, thereby stabilising the complex under strongly acidic conditions by protecting
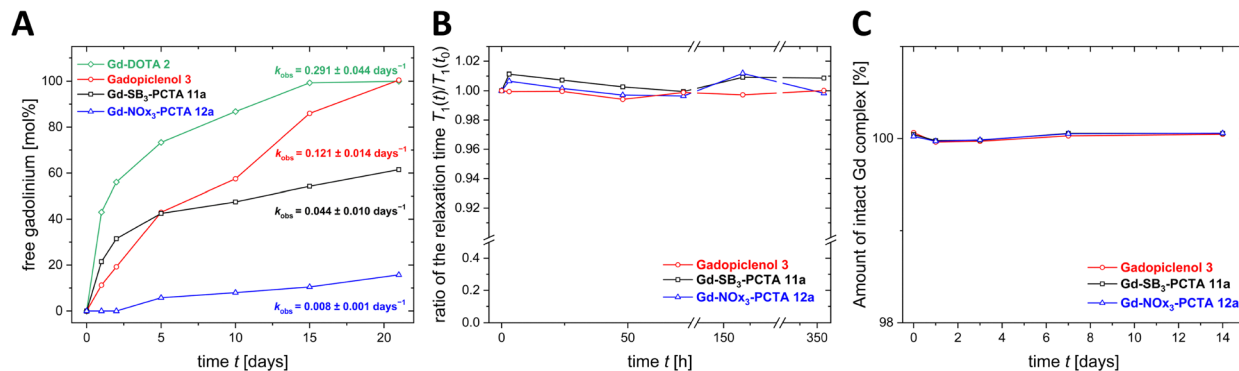
Fig. 2 (A) Released free gadolinium over time for Gd-SB$_3$-PCTA **11a**, Gd-NOx$_3$-PCTA **12a**, gadopiclenol **3** and Gd-DOTA **2** under acidic conditions (pH 1.2) at 37 °C, as determined by complexometric titration with arsenazo III. (B) Time-dependent relative longitudinal relaxation time $T_1(t)/T_1(t_0)$ of gadolinium complexes (1.25 mM) in presence of ZnCl$_2$ (1.25 mM) in phosphate-buffered saline (PBS, pH 7.4, 37 °C), measured at 1.4 T. Measurements were performed at 0 h, 3 h, 1 day, 3 days, 7 days and 15 days. (C) Stability of Gd(III) complexes in human serum at 37 °C. Measurements were performed at 0 days, 1 day, 3 days, 7 days and 14 days.

the macrocyclic coordination center from protonation and subsequent Gd(III) release.

In contrast to the *in vitro* evaluation of kinetic stability, the assessment of thermodynamic stability of GBCAs is more challenging, as it cannot be easily extrapolated to *in vivo* conditions due to the complex composition of biological media, containing numerous competing endogenous complex ligands and metal cations (*e.g.* Fe(III), Ca(II), Zn(II), Cu(II)).[32,33] Upon decomplexation, free Gd(III) may bind to proteins or precipitate with endogenous anions.[34] A robust and widely accepted method for evaluating GBCA stability under physiologically relevant conditions involves transmetalation with Zn(II) in phosphate buffer.[16,33,35] The zwitterionic complexes Gd-SB$_3$-PCTA **11a** and Gd-NOx$_3$-PCTA **12a** as well as gadopiclenol as non-zwitterionic reference were challenged with excess Zn(II) in phosphate-buffered saline (PBS, pH 7.4) at 37 °C. Longitudinal relaxation rates were monitored at the following time points: 0 h, 3 h, 1 day, 3 days, 7 days and 15 days. It is important to note that the Zn(II) solution must be freshly prepared with ZnCl$_2$ and added immediately to the chelator solutions to avoid the formation of zinc phosphate precipitates.[32] The zwitterionic complexes Gd-SB$_3$-PCTA **11a** and Gd-NOx$_3$-PCTA **12a**, as well as gadopiclenol **3**, showed no signs of instability as the measured longitudinal relaxation rates remained constant throughout the observation period of 15 days. These results are consistent with previous studies of gadopiclenol[16] and suggest that Gd-SB$_3$-PCTA **11a** and Gd-NOx$_3$-PCTA **12a** are at least as stable as gadopiclenol **3** against transchelation.

These observations were further confirmed by a stability assay in human serum at 37 °C. All Gd(III) complexes were incubated for 15 days and gadolinium release was quantified at 0 h, 1 day, 3 days, 7 days and 15 days by complexometric titration with Arsenazo III. No loss of Gd(III) was observed for any of the zwitterionic complexes Gd-SB$_3$-PCTA **11a** and Gd-NOx$_3$-PCTA **12a** or for gadopiclenol **3**. The molecular integrity of Gd-SB$_3$-PCTA **11a** and Gd-NOx$_3$-PCTA **12a** was verified after 15 days of incubation *via* LC/MS. At least in serum, we have thus no evidence for reductive biotransformation of the *N*-oxide **12a**.

This fact is notable because certain amineoxides have been reported to be reduced in biological media.[36]

Relaxivity at 1.4 T and 7 T

The relaxivity of GBCAs depends on several factors, including hydration number q, the mean residence time of inner-sphere water molecules, the electronic relaxation time and the rotational correlation time of the complex.[37,38] Relaxivity arises from the combined contributions of inner-sphere (IS) and outer-sphere (OS) interactions, as described by the following equation: $R_1 = R_{1,\text{inner-sphere}} + R_{1,\text{outer-sphere}}$. Here $R_{1,\text{inner-sphere}}$ refers to the longitudinal relaxation rate originating from inner-sphere interactions and $R_{1,\text{outer-sphere}}$ accounts for the contribution from outer-sphere interactions. The inner-sphere component refers to the relaxation of water molecules directly bound to the Gd(III) ion, whereas the outer-sphere contribution results from transient interactions between the complex and bulk water molecules not directly bound to the metal centre. An effective strategy to enhance the longitudinal relaxation rate R_1 is to increase the inner-sphere contribution by raising the hydration number q. According to the Solomon–Bloembergen–Morgan (SBM) theory, R_1 is directly proportional to the hydration number q: $R_{1,\text{inner sphere}} = \dfrac{q_{\text{Gd}}[\text{GBCA}]}{[\text{H}_2\text{O}]}\dfrac{1}{T_{1\text{m}} + \tau_{\text{m}}}$ where q_{Gd} refers to the number of inner-sphere water molecules coordinated per Gd(III), [GBCA] is the concentration of the contrast agent, [H$_2$O] is the bulk water concentration, $T_{1\text{m}}$ is the longitudinal relaxation time of the inner-sphere water protons and τ_{m} is the mean residence time of these coordinated water molecules.[39]

Another key factor contributing to the overall relaxivity of a GBCA is the outer-sphere component, which can be modulated by parameters such as molecular size, rotational correlation time and electronic relaxation time.[38,39] As small molecules, GBCAs typically exhibit rapid rotational diffusion, which limits their relaxivity. The outer-sphere contribution can be enhanced by increasing the hydrodynamic size of the complex, thereby

reducing its rotational correlation time and resulting in higher relaxivity. For gadopiclenol 3, Robic *et al.* proposed that the isoserinol arms contribute to an increased hydrodynamic size.[16] In parallel, based on the observations by Botta *et al.* a second coordination sphere contribution has been suggested, as the highly polar polyhydroxy groups may enhance the number of water molecules associated to the complex.[22] These observations are further supported by the findings of Holzapfel *et al.* on chiral DOTA-based complexes with $q = 1$.[20] It was demonstrated that not only the spatial expansion of the complex through the introduction of side arms significantly influences relaxivity, but also the incorporation of zwitterionic and highly hydrophilic moieties has a substantial impact on the observed high relaxivity.[20]

Relaxometric studies of the two novel zwitterionic GBCAs Gd-SB$_3$-PCTA **11a** and Gd-NOx$_3$-PCTA **12a** were performed at two different and clinically relevant field strengths (1.4 T and 7 T). The longitudinal relaxivity r_1 of both zwitterionic complexes, in comparison with gadopiclenol as a reference, was investigated at a field strength of 1.4 T (60 MHz, 37 °C, water) using a standard inversion-recovery pulse sequence. The spin lattice relaxation time (T_1) was determined and plotted as the reciprocal ($1/T_1$) against the concentration of the respective complexes. The concentrations

of the complexes were precisely determined by inductively coupled plasma mass spectrometry (ICP-MS).

For Gd-SB$_3$-PCTA **11a** a longitudinal relaxivity of $r_{1,1.4T} = 16.29 \pm 0.22$ mM^{-1} s^{-1} was observed, representing an 18% increase compared to gadopiclenol ($r_{1,1.4T} = 13.82 \pm 0.05$ mM^{-1} s^{-1}). Gd-NOx$_3$-PCTA **12a** had a slightly lower relaxivity of $r_{1,1.4T} = 12.69 \pm 0.07$ mM^{-1} s^{-1}, representing an 8% decrease compared to gadopiclenol (Fig. 3).

To evaluate the field dependence of relaxivity, additional measurements were conducted at 7 T (300 MHz, room temperature, water), a magnetic field strength increasingly relevant in preclinical and high-resolution clinical imaging. These measurements were performed using a preclinical MR imager by measuring a slice-selective 2D inversion recovery spin echo sequence with inversion times ranging from 50 ms to 3200 ms (Fig. 3).

Both zwitterionic complexes showed a magnetic field dependence comparable to gadopiclenol, maintaining high relaxivity values even at 7 T. For Gd-SB$_3$-PCTA **11a** a longitudinal relaxivity of $r_{1,7T} = 14.28 \pm 0.22$ mM^{-1} s^{-1} was measured, while Gd-NOx$_3$-PCTA **12a** exhibited a relaxivity of $r_{1,7T} = 9.98 \pm 0.17$ mM^{-1} s^{-1}. Compared to the values at 1.4 T this corresponds to a field dependent relaxivity reduction of 12% for Gd-SB$_3$-PCTA **11a**,
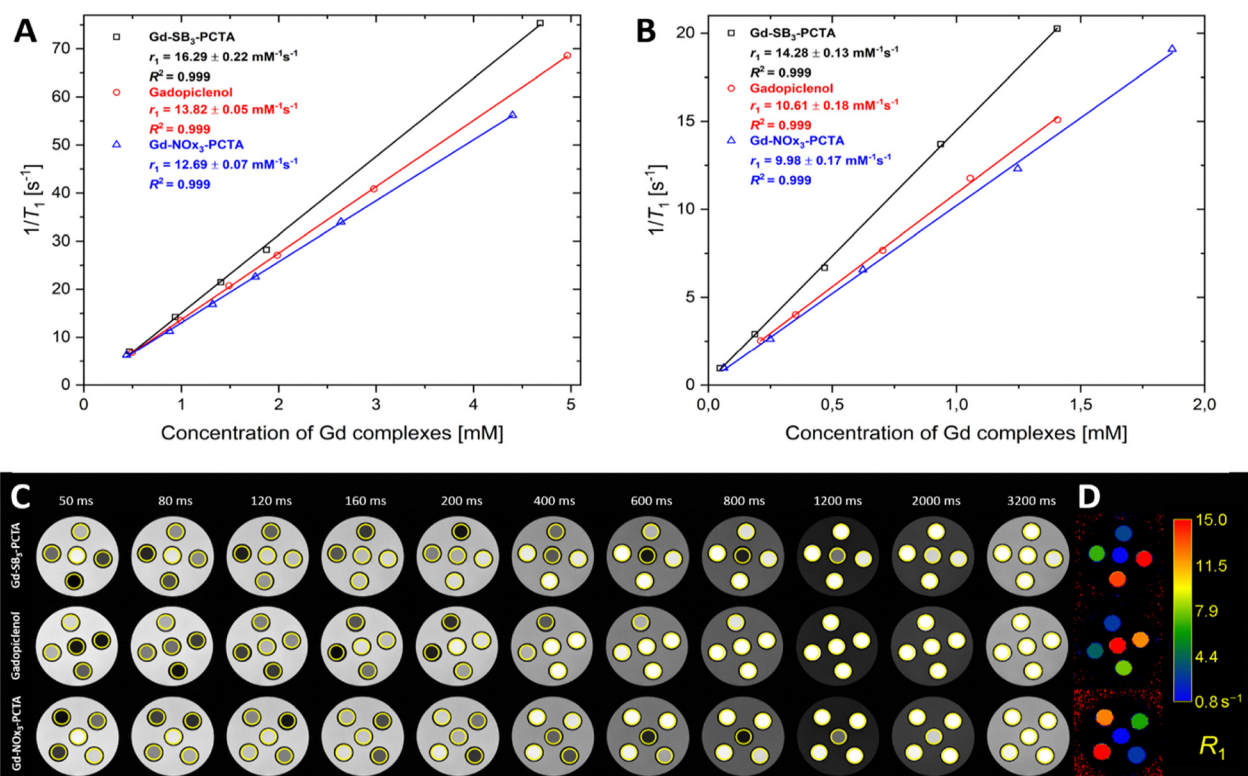

Fig. 3 (A) Longitudinal relaxivity (r_1) determined from plotting the reciprocal relaxation time $1/T_1$ *versus* the concentration of Gd-SB$_3$-PCTA **11a**, Gd-NOx$_3$-PCTA **12a** and gadopiclenol **3** in H$_2$O at 37 °C and 1.4 T (60 MHz) (B) longitudinal relaxivity (r_1) determined from plotting the reciprocal relaxation time $1/T_1$ *versus* the concentration of Gd-SB$_3$-PCTA **11a**, Gd-NOx$_3$-PCTA **12a** and gadopiclenol **3** in H$_2$O at room temperature and 7 T (300 MHz) (C) representative MR images acquired at 7 T at multiple inversion times (TI) ranging from 50 ms to 3200 ms of Gd-SB$_3$-PCTA **11a**, Gd-NOx$_3$-PCTA **12a** and gadopiclenol **3** in a phantom holder and surrounded by water. Yellow circles represent the regions of interest for five different concentrations of each compound used for subsequent quantitative analysis. (D) Color-coded R_1 relaxation rate map acquired at 7 T with an inversion-recovery spin-echo sequence with multiple inversion time delays for five different concentrations of each compound.

Table 1 Molecular weights, longitudinal relaxivity (r_1) values at 1.4 T and 7 T and q values for Gd-SB$_3$-PCTA **11a**, Gd-NOx$_3$-PCTA **12a**, gadopiclenol **3**, Gd-PCTA and Gd-DOTA **2**

Parameter	Gd-SB$_3$-PCTA	Gd-NOx$_3$-PCTA	Gadopiclenol	Gd-PCTA	Gd-DOTA
M [g mol^{-1}]	1357.39	1039.23	970.10	534.63	558.64
$r_{1,1.4T}$ [mM^{-1} s^{-1}]	16.29 ± 0.22^a	12.69 ± 0.07^a	13.82 ± 0.05^a	4.9^{de}	3.3^{de}
$r_{1,7T}$ [mM^{-1} s^{-1}]	14.28 ± 0.13^b	9.98 ± 0.17^b	10.61 ± 0.18^b (10.68^f)	—	—
q	2.08^c	2.23^c	2^e	2^e	1^e

^{a} H$_2$O, 37 °C. ^{b} H$_2$O, room temperature. ^{c} Determined *via* luminescence lifetime measurements of the Eu(III) complexes. ^{d} 1.5 T, 37 °C. ^{e} Napolitano *et al.*[19] ^{f} Robic *et al.*[16]

23% for gadopiclenol **3** and 21% for Gd-NOx$_3$-PCTA **12a** (Table 1).

In summary, Gd-SB$_3$-PCTA **11a** has a consistently higher relaxivity than the benchmark GBCA gadopiclenol **3** at a magnetic field strength of 1.4 and 7 T. Its superior performance is attributed to enhanced hydration caused by the sulfobetaine side chains, which appear to provide more effective kosmotropicity than the polar isoserinol sidechains present in gadopiclenol **3**. This gain in hydration likely contributes not only to a larger hydrodynamic radius, thereby slowing rotational diffusion, but may also promote dynamic equilibria involved in inner-sphere und outer-sphere processes.

Structure-stability relationships of zwitterionic Gd-PCTA complexes

As mentioned above, Gd-NOx$_3$-PCTA **12a** has a slightly lower relaxivity compared to Gd-SB$_3$-PCTA **11a** and gadopiclenol **3**. An influence of the stereochemistry as proposed by Napolitano *et al.*[19] for stereoisomers of gadopiclenol can be excluded here, because both derivatives Gd-NOx$_3$-PCTA **12a** and Gd-SB$_3$-PCTA **11a** are based on the same (enantiomerically pure) scaffold. Instead, two other possible explanations come to mind: (1) the *N*-oxide sidechain functionalities might contribute to Gd-coordination, which could reduce the number of inner-sphere water molecules to $q < 2$ (Scheme 2). This effect would reduce the relaxivity of Gd-NOx$_3$-PCTA **12a** and could also explain the high stability of this complex under acidic conditions. The process is not unlikely because *N*-oxides are good complex ligands for oxophilic metals.[40] Sulfobetaines in turn are only weak ligands, which would explain the difference to Gd-SB$_3$-PCTA **11a**. (2) The difference in relaxivity might be due to the more compact molecular structure of Gd-NOx$_3$-PCTA **12a** as a consequence of the small *N*-oxide groups. Molecular size and

shape have an impact on the relaxation properties of GBCAs explaining the reduced relaxivity of Gd-NOx$_3$-PCTA **12a**.

To check the first hypothesis mentioned above, the hydration number q was determined according to the method described by Beeby *et al.* and Supkowski *et al.*[29,41] For this purpose, the luminescence lifetimes τ of the corresponding Eu(III) complexes, Eu-SB$_3$-PCTA **11b** and Eu-NOx$_3$-PCTA **12b**, were measured in both H$_2$O and D$_2$O.

The hydration number q was then calculated using the following equation $q = 1.11\left(\left(\dfrac{1}{\tau_{H_2O}}\right) - \left(\dfrac{1}{\tau_{D_2O}}\right) - 0.31\right)$ where $\tau(H_2O)$ represents the excited-state lifetimes in H$_2$O and $\tau(D_2O)$ in D$_2$O.

The values obtained are given in Table 2. They reveal that both Eu(III) complexes have almost the same hydration number $q \sim 2$. Displacement of an inner-sphere water molecule by one of the *N*-oxide side chain groups is therefore not responsible for the lower relaxivity of Gd-NOx$_3$-PCTA **12a**. Instead, the more compact molecular structure of the *N*-oxide **12a** compared to sulfobetaine **11a** explains the slightly lower relaxivity.

In vivo gadolinium kidney retention

In a first attempt to assess the impact of zwitterionic modifications on *in vivo* Gd(III) retention, mice were treated with the most promising zwitterionic GBCA Gd-SB$_3$-PCTA **11a** and gadopiclenol **3** as a current clinical reference, in analogy to an *in vivo* study design reported by Di Gregorio *et al.* (Fig. 4).[42] Animals received ten consecutive doses of 0.1 mmol kg^{-1}, corresponding to a cumulative dose of 1 mmol kg^{-1}. After a 17-day clearance phase following the last administration organs were harvested and analysed. Previous studies revealed the highest retentions of Gd(III) after GBCA administration in the kidney cortex of both animals and humans.[11,43] The impact of a long-term Gd(III) retention in the kidney on patient health is unclear, but certainly an undesirable side effect of clinical GBCA use. The residual renal Gd(III) content was therefore quantified by ICP-MS, revealing amounts of 5.89 ± 0.26 nmol g^{-1} Gd(III) for
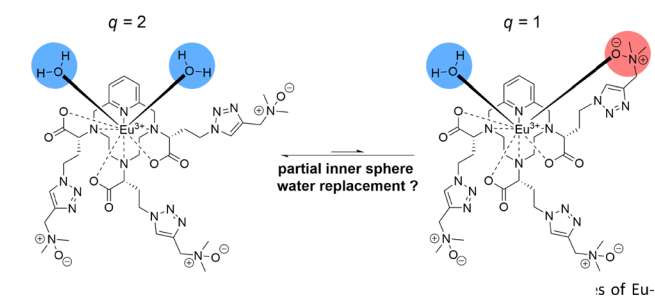
Scheme 2 Proposed equilibrium between the $q = 2$ and $q = 1$ hydration states of Eu-NOx$_3$-PCTA **12b**.

Table 2 Luminescence lifetimes τ and hydration numbers q of Eu-SB$_3$-PCTA **11b** and Eu-NOx$_3$-PCTA **12b**, determined by time-resolved emission spectroscopy in H$_2$O and D$_2$O

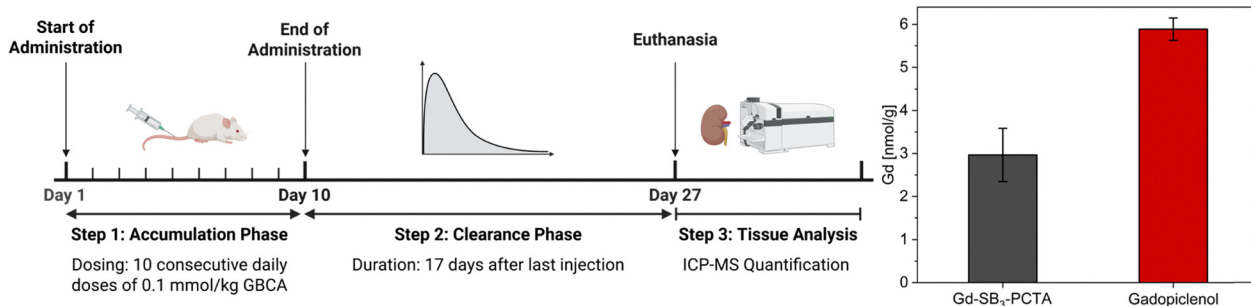| Complex	$\tau(H_2O)$ [ms]	$\tau(D_2O)$ [ms]	q
Eu-SB$_3$-PCTA **11b**	0.348 ± 0.002	1.445 ± 0.012	2.08
Eu-NOx$_3$-PCTA **12b**	0.357 ± 0.0006	2.061 ± 0.021	2.23

Fig. 4 Study design of the *in vivo* kidney retention of Gd-SB$_3$-PCTA **11a** and gadopiclenol **3** with a total dose of 1 mmol kg^{-1} and a clearance phase of 17 days after last administration and Gd(III) retention in the kidney of animals treated with **3** and **11a** as measured by ICP-MS.

the reference compound gadopiclenol **3** and 2.97 ± 0.62 nmol g^{-1} for the zwitterionic derivative Gd-SB$_3$-PCTA **11a**. The introduction of zwitterionic groups led thus to a reduction of kidney gadolinium retention of 50%.

Conclusion

GBCAs are an important component of clinical diagnostics using MRI. However, the long-term Gd(III) retention in patients treated repeatedly with GBCAs has led to safety concerns. The next generation of GBCAs should therefore have the highest possible relaxivity (enabling low dosage), high complex stability (no release of Gd(III) *in vivo*), and the lowest possible gadolinium retention in patients.

This study describes the synthesis of novel zwitterionic GBCAs based on the chelator PCTA. Bn$_3$-PCTAZA **8** is a central intermediate bearing three azide groups for CuAAC. The alkylation of pyclen gave the stereoisomerically pure (*R,R,R*)-configured product. Compared to other known protocols for the preparation of chiral PCTA derivatives, this eliminates the laborious separation of stereoisomers after synthesis. Sulfobetaines and *N*-oxides were introduced as zwitterionic groups *via* a CuAAC reaction. The resulting complexes Gd-SB$_3$-PCTA **11a** and Gd-NOx$_3$-PCTA **12a** have high thermodynamic and kinetic stability, superior to that of gadopiclenol **3** (the most stable clinically used GBCA). The complexes **11a** and **12a** are exceptionally stable in acidic media (pH 1.2 for days), in human serum, and towards transmetalation with Zn(II).

The hydration number was determined to be *q* ∼ 2 for both zwitterionic compounds based on the luminescence lifetime of corresponding Eu(III) complexes **11b** and **12b**. The resulting relaxivities of the zwitterionic GBCAs Gd-SB$_3$-PCTA **11a** and Gd-NOx$_3$-PCTA **12a** are therefore much higher than those of the clinically frequently used gadoteric acid. With a relaxivity of $r_{1,1.4T} = 16.29 \pm 0.22$ mM^{-1} s^{-1}, the sulfobetaine **11a** has a 18% higher relaxivity than gadopiclenol **3** (currently the clinically used GBCA with the highest relaxivity). The increased relaxivity compared to gadopiclenol is likely due to the strong hydration of the zwitterions, which increases the hydrodynamic diameter of the compounds. The decoration of the GBCAs with zwitterions also led to a 50% reduction in gadolinium deposition in the kidneys of mice treated repeatedly with **11a** compared to gadopiclenol **3**.

Our study has several limitations, which need to be addressed in future work. NMRD measurements could shed more light on the contribution of zwitterionic groups on inner- and outer-sphere effects influencing relaxivity. *In vivo* experiments have been restricted to a small cohort of animals and sex differences have not been addressed so far. A more comprehensive analysis of the biodistribution is therefore needed.

However, the results obtained suggest that zwitterionic GBCAs such as Gd-SB$_3$-PCTA **11a** and Gd-NOx$_3$-PCTA **12a** have the potential to serve as safer contrast agents for MRI with high stability, high relaxivity, and low renal Gd(III) retention.

Experimental section

General

The sulfobetaine alkyne **14** was synthesised according to the procedure reported by Niu *et al.*, while the synthesis of the alkyne *N*-oxide **15** has also been previously described in the literature.[44] In our hands, the most reliable method for obtaining a stable and analytically pure form of the alkyne *N*-oxide **15** involved the oxidation of *N,N*-dimethylpropargylamine (**13**) with *meta*-chloroperoxybenzoic acid (*m*CPBA) following a modified version of the procedure reported by Galán *et al.*[45] As the alkyne *N*-oxide **15** has been reported to be unstable even at low temperatures but was found to be stable in aqueous solution, we recommend immediate dissolution in water upon isolation, yielding a 3 M aqueous stock solution. This solution proved to be stable at 4 °C over at least two months and provided a convenient concentration for CuAAC reactions in mixed DMF/H$_2$O systems, in which all reactants were sufficiently soluble. All commercially available reagents and starting materials were purchased from Sigma Aldrich, TCI, abcr or BLDpharm and were used without further purification. Gadopiclenol **3** was purchased as Vueway® from Bracco Imaging SpA as a 0.5 mmol mL^{-1} aqueous solution. Non-deuterated solvents in HPLC grade were purchased from VWR chemicals and deuterated solvents were purchased from Deutero GmbH. Water was purified using an ELGA PURELAB Classic UV water system. Reactions were monitored *via* HPLC-MS or TLC (Macherey Nagel TLC aluminum sheets, ALUGRAMSIL G UV254, 2.5 cm × 7.5 cm). Spots were

visualized under UV light and/or by staining with a basic aqueous KMnO$_4$ solution.

Medium pressure liquid chromatography was performed on automated systems using prepacked cartridges (Interchim). For the use of alkaline alumina an empty cartridge was filled with alkaline alumina for chromatography. Normal phase chromatography was performed using a Biotage Isolera Prime system and for reversed flash chromatography an Interchim PuriFlash 430 system with MeCN/H$_2$O containing 0.1% formic acid as the mobile phase.

NMR analyses were performed on Bruker Avance III HD 600 MHz and Bruker Avance I 400 MHz spectrometers. Chemical shifts (δ) are expressed in parts per millions (ppm). High-resolution mass spectrometry (HRMS) was performed on an Agilent 6230 ESI-TOF coupled with an Agilent HPLC 1200 series HPLC system.

Analytical HPLC-MS was performed on an Agilent HPLC system 1260 Infinity II with a Macherey Nagel NUCLEODUR C18 Gravity-SB, 3 μm, 100 × 2 mm column linked to a Bruker Ion Trap mass spectrometer with an ESI ionization source.

Relaxivity measurements at 1.4 T

The determination of the longitudinal relaxivity at 60 MHz (1.4 T) was conducted based on the spin lattice relaxation time (T_1) using a Bruker Minispec mq60 analyzer at 37 °C. T_1 measurements were performed using the standard inversion recovery pulse sequence (180°–τ–90°) at a temperature of 37 °C ± 0.1 °C. For each measurement 20 unevenly spaced data points were acquired after inversion times between 5 ms and 400 ms. r_1 was obtained by plotting the inverse relaxation time $1/T_1$ *versus* the concentration of the complexes and slope determination *via* the linear regression function in OriginLab 2022. The concentration of the complexes was determined *via* ICP-MS of the highest sample concentration.

Relaxivity measurements at 7 T

Relaxation time measurements at 7 T were conducted using a preclinical MRI scanner (Bruker Biospec 70/30, Ettlingen) at room temperature with a volume receive coil of an inner diameter of 40 mm. Five PCR tubes containing each 320 μL volume of different aqueous sample solutions (0.05–2 mM) were positioned in a holder within a 50 mL Falcon tube filled with water, aligned parallel to the magnet bore. All imaging sequences utilized transversal orientation.

Following an initial survey scan, two distinct T_1-measurement protocols were implemented. A 2D Look Locker EPI-based sequence provided quick qualitative visual T_1 inspection within 4 minutes. This protocol employed inversion times (TI) ranging from 20 to 770 ms in 50 ms increments, with TR 5000 ms and TE 9.9 ms. K-Space acquisition utilized six segments with 8 averages, 10° RF pulses, and a 200 kHz readout bandwidth. Imaging parameters included a 32 mm field of view, 128 × 128 matrix, and 1.2 mm slice thickness.

Subsequently, a slice-selective 2D inversion recovery spin echo sequence was acquired over approximately 2 hours. This protocol incorporated eleven inversion times (50, 80, 120, 160,

200, 400, 600, 800, 1200, 2000, and 3200 ms) with TE 7.0 ms, TR 5000 ms, and an 80 kHz readout bandwidth. Three slices of 1 mm thickness were obtained with 0.5 mm inter-slice gaps and 30 mm field of view with a 128 × 128 matrix.

Relaxation time analysis was conducted using qMapIt, an in-house quantification software that extends ImageJ functionality. Inversion recovery datasets underwent model function fitting:

$$\text{Signal}_{\text{TI}} = A \times \frac{1 + e^{(-R_1 \times \text{TI})} - 2 \times e^{(-R_1 \times \text{TR})}}{1 - 2 \times e^{(-R_1 \times \text{TR})}} \quad \text{(eqn (4))}$$

with $T_1 = R_1^{-1}$ *via* a nonlinear least-squares Dog–Leg algorithm, generating amplitude A and relaxation time T_1 maps. The inversion recovery data was smoothed before fitting with a Median filter of 0.5 pixel to reduce Gibbs-ringing.

Automated contour detection identified individual tube boundaries, with segmented regions stored as regions of interest (ROIs) for subsequent quantitative analysis. The complete analytical workflow was orchestrated through a Python script executed within a Jupyter notebook environment, which seamlessly integrated Fiji and qMapIt operations *via* PyImageJ.

Inductively coupled plasma mass spectrometry (ICP-MS)

Gadolinium concentrations were determined by inductively coupled plasma mass spectrometry (ICP-MS). Prior to ICP-MS measurements, 10 μL of the samples were digested in 1 mL of nitric acid (ROTIPURAN® Supra, 69%) for 24 h at room temperature in pre-cleaned tubes. Afterwards, all samples were filled up to 12 mL with ultrapure water. The digested samples were then diluted 1 : 100 prior to analysis. The measurements were performed on an Agilent Technologies 7800x ICP-MS (Agilent Technologies Inc., Santa Clara, USA) equipped with a quadrupole mass analyzer. Prior to measurement, the ICP-MS setup was tuned with a mixture of Ce, Co, Li, Tl and Y at a concentration of 1 ppb (Agilent Technologies Inc., Santa Clara, USA). External calibration was performed using mixed element standards purchased from Merck KGaA and PerkinElmer® Inc. Calibration solutions containing Gd at concentrations of 0 to 1000 ppb were prepared freshly. Quantitation was performed by external calibration, corrected by internal standard (115 In for Gd). To ensure stability during the measurement a quality control sample containing 1 ppb Gd was measured.

Kinetic stability in acidic medium

The kinetic stability of the complexes was evaluated by incubating aqueous solutions (8 μmol L^{-1}) of the Gd(III) complexes in hydrochloric acid (pH 1.2) at 37 °C. The Gd(III) concentration of the solutions was confirmed by ICP-MS. The extent of decomplexation was quantified *via* UV-vis spectroscopy following complexometric titration with Arsenazo III. For each measurement a 1 mL aliquot of the acidic solution was mixed with 39 μL of an aqueous Arsenazo III solution (0.53 mmol L^{-1}) and 100 μL of an aqueous sodium acetate solution (1 mol L^{-1}). Following the absorption at 654 nm was measured using a 1 cm quartz cuvette at time points 1 day, 2 days, 5 days, 10 days, 15 days and 21 days.

Transmetallation/dechelation stability assay in the presence of phosphate and Zn²⁺

Pre-warmed to 37 °C solutions of the Gd(III) complexes (2.5 mM) and ZnCl₂ (2.5 mM) in aqueous 1 × PBS buffer (pH 7.4) were mixed in a 1 : 1 ratio and the spin lattice relaxation time T_1 was measured immediately to define the time point $t = 0$ min. The mixtures were then incubated at 37 °C and T_1 was recorded at 3 h, 1 day, 2 days, 3 days, 7 days and 15 days. All T_1 measurements were performed at 37 °C ± 0.1 °C using a Bruker Minispec mq60 analyser employing the standard inversion recovery pulse sequence. The T_1 values were subsequently plotted as a ratio relative to the initial value measured at $t = 0$ min.

Stability in human serum at 37 °C

The stability of the Gd(III) complexes was evaluated by incubating a solution of the complexes in human serum at 37 °C using a thermocycler followed by komplexometric determination with Arsenazo III. Human serum (Capricorn Scientific, male, type AB) was supplemented with sodium azide (1.7 mmol L⁻¹) as a microbial inhibitor prior to use. For each measurement, a 50 μL aliquot of the incubation mixture was diluted with 950 μL H₂O to obtain a final concentration of 8 μmol L⁻¹ of total gadolinium. Subsequently, 39 μL of an aqueous Arsenazo III solution (0.53 mmol L⁻¹) were added and the amount of free Gd(III) was quantified as described above. Measurements were performed at defined time points (0 h, 1 day, 3 days, 7 days and 14 days).

Luminescence lifetime measurements and q value determination

Excitation, emission and lifetime measurements were performed on an Agilent Cary Eclipse fluorescence spectrometer using a 1 cm quartz cell. Luminescence decay was recorded with an excitation wavelength of $\lambda_{exc} = 271$ nm and an emission wavelength of $\lambda_{em} = 615$ nm. The luminescence lifetime was determined by monoexponential fitting of the data in OriginLab 2022. Hydration numbers q were calculated following the protocol by Beeby et al. and Supkowski et al.[29,41]

In vivo kidney retention study

All animal experiments described in this manuscript were conducted in accordance with the ARRIVE guidelines (https://www.nc3rs.org.uk/arrive-guidelines) and protocols were approved by the Institutional Animal Care and Use Committee (IACUC) of Washington University in St. Louis. The laboratory conducting the experiments is accredited under protocol number 24-0832-02.

For in vivo evaluation of renal gadolinium retention male C57BL/6J mice ($n = 2$, 10–12 weeks, 25–30 g) received 10 consecutive intravenous injections of gadopiclenol **3** and Gd-SB₃-PCTA **11a** via the tail vein at 0.1 mmol kg⁻¹ each (100 μL, saline, pH 7.4) over 10 days. Seventeen days after the final administration, animals were euthanised, organs were harvested and kept frozen until organ digestion and ICP-MS analysis was performed as described in the following. All animals showed no changes in body weight or behaviour following compound administration.

Kidney digestion and ICP-MS analysis

Kidneys ($n = 2$) were transferred into pre-cleaned tubes, weighed and spiked with dysprosium as internal standard (Thermo Fisher Specpure™, Dy plasma standard, 1008 ± 8 μg mL⁻¹) to reach 100 μg L⁻¹ in the final solution used for ICP-MS. For digestion, 2 mL of nitric acid (ROTIPURAN® Supra, 69%) were added and samples were incubated at 37 °C for 18 h. The digests were diluted to 10 mL with MilliQ H₂O, followed by a 1 : 2 dilution. To remove residual particulates, the solutions were centrifuged at 3500 × g for 15 min, decanted and subsequently analysed by ICP-MS in triplicates under the same conditions as described before.

Synthesis

Triflate 6. To a solution of (S)-benzyl-4-azido-2-hydroxybutanoat (**5**) (1.54 g, 6.57 mmol, 1.00 eq.) in CH₂Cl₂ (65 mL) at −20 °C was added 2,6-lutidine (1.14 mL, 9.85 mmol, 1.50 eq.) followed by the dropwise addition of trifluoromethanesulfonic anhydride (1.55 mL, 9.20 mmol, 1.40 eq.). During the addition the solution became orange, then redish. The solution was stirred at −20 °C for 1 h, the cooling bath was switched to an ice bath and the solution was stirred at 0 °C for 1 h. All volatiles were removed in vacuo (water bath: room temperature) and the crude product was obtained as a yellowish oil. The crude product was purified via flash chromatography (loaded as solution in CH₂Cl₂ (6 mL), 30 μm spherical silica gel, Interchim cartridge F0040, 100% CH₂Cl₂ isocratic). (S)-Benzyl-4-azido-2-(triflyloxy)-butanoate (**2**) (2.32 g, 96%) was obtained as an orangeish oil. ¹H-NMR (CDCl₃, 600 MHz) δ = 7.41–7.36 (5H, m, Ph-H̲), 5.30–5.26 (3H, m, Ph-CH̲₂, BnO₂C-CH̲), 3.54–3.42 (2H, m, CH̲₂-CH₂-N₃), 2.28–2.19 (2H, m, CH̲₂-CH₂-N₃).¹⁹F-NMR (CDCl₃, 564 MHz) δ = −74.7 (OTf).

(R,R,R)-Bn₃-PCTAZA 8. To a solution of pyclen **7** (273 mg, 1.32 mmol, 1.00 eq.) in anhydrous MeCN (10 mL) was added Cs₂CO₃ (1.51 g, 4.63 mmol, 3.50 eq.) and the suspension was cooled via an ice bath. Following a solution of (S)-benzyl-4-azido-2-(triflyloxy)-butanoate (**6**) (1.60 g, 4.37 mmol, 3.30 eq.) in anhydrous MeCN (25 mL) was added dropwise over 30 min. The reaction mixture was warmed to room temperature and stirred at this temperature for 2 h. Afterwards the solvent was removed in vacuo and the residue was dissolved in sat. aq. NaHCO₃ solution (30 mL) and CH₂Cl₂ (40 mL). The phases were separated and the aq. phase was extracted with CH₂Cl₂ (3 × 30 mL). The combined org. phases were dried over Na₂SO₄, the solvent was removed in vacuo and the crude product was obtained as an orange oil. The crude product was purified via flash chromatography (loaded as solution in CH₂Cl₂ (4 mL), 15 μm spherical silica gel, Interchim cartridge F0040, 100% CH₂Cl₂ for 1 CV then gradient to 100% MeCN in 10 CV, 100% MeCN for 3 CV). (R,R,R)-Bn₃-PCTAZA **8** (1.11 g, 98%) was obtained as an orangeish viscous oil. Rf (CH₂Cl₂/MeOH/Et₃N 95 : 4.5 : 0.5) = 0.60. HRMS (ESI) m/z [M+H]⁺ calcd for C₄₄H₅₂N₁₃O₆⁺: 858.4158, found: 858.4117. ¹H-NMR (CDCl₃, 600 MHz) δ = 7.60 (1H, t, ³$J_{H,H}$ = 7.7 Hz, C_pyridine-H̲_para to N_pyridine), 7.41–7.27 (15H, m, CH₂-Ph-H̲),7.10 (2H, d, ³$J_{H,H}$ = 7.6 Hz, C_pyridine-H̲ meta to

$N_{pyridine}$), 5.22 (2H, d, $^2J_{H,H}$ = 12.5 Hz, Ph-C$\underline{H}_2$-), 5.18 (2H, d, $^2J_{H,H}$ = 12.3 Hz, Ph-C$\underline{H}_2$-), 5.03 (2H, s, Ph-C$\underline{H}_2$-), 3.94 (2H, d, $^2J_{H,H}$ = 11.9 Hz, Py-C$\underline{H}_2$-N), 3.75 (2H, d, $^2J_{H,H}$ = 11.9 Hz, Py-C$\underline{H}_2$-N), 3.52 (2H, m, BnO$_2$C-C$\underline{H}$- next to pyridine), 3.46–3.35 (4H, m, C$\underline{H}_2$-CH$_2$-N$_3$ sidearms next to pyridine), 3.21–3.14 (3H, m, BnO$_2$C-C$\underline{H}$ opposite pyridine, C$\underline{H}_2$-CH$_2$-N$_3$ sidearm opposite pyridine), 2.90–2.81 (3H, m, C$\underline{H}_2$-CH$_2$-N$_3$), 2.20–2.13 (3H, m, CH$_2$-C$\underline{H}_2$-N$_3$), 2.12–1.98 (3H, m, N-C$\underline{H}_2$-CH$_2$-N, N-CH$_2$-C(H)H-N), 1.93–1.85 (2H, m, N-C$\underline{H}_2$-CH$_2$-N), 1.84–1.78 (1H, m, N-CH$_2$-C(H)H-N), 1.57–1.52 (1H, m, N-CH$_2$-C(H)H-N), 1.32–1.26 (1H, m, N-CH$_2$-C(H)H-N). ^{13}C-NMR (CDCl$_3$, 150 MHz) δ = 172.9 (C$_{carbonyl}$ sidearm opposite pyridine), 172.4 (C$_{carbonyl}$ sidearms next to pyridine), 158.3 (quart. C$_{pyridine}$), 137.6 (quart. C$_{phenyl}$), 135.9 (C$_{para}$ to N$_{pyridine}$), 128.9 (C$_{phenyl}$), 128.8 (C$_{phenyl}$), 128.7 (C$_{phenyl}$),128.6 (C$_{phenyl}$), 128.5 (C$_{phenyl}$), 128.4 (C$_{phenyl}$), 122.9 (C$_{meta}$ to N$_{pyridine}$), 66.6 (Ph-C$\underline{H}_2$ sidearms next to pyridine), 66.3 (Ph-C$\underline{H}_2$ sidearm opposite pyridine), 63.8 (BnO$_2$C-C$\underline{H}$-, sidearms next to pyridine), 63.0 (BnO$_2$C-C$\underline{H}$-, sidearm opposite pyridine), 57.9 (pyridine-C$\underline{H}_2$-), 52.9 (C$\underline{H}_2$-CH$_2$-N$_3$), 50.5 (C$\underline{H}_2$-CH$_2$-N$_3$), 48.4 (CH$_2$-C$\underline{H}_2$-N$_3$ sidearms next to pyridine), 48.3 (CH$_2$-C$\underline{H}_2$-N$_3$ sidearm opposite pyridine), 30.0 (N-C$\underline{H}_2$-CH$_2$-N), 29.8 (N-C$\underline{H}_2$-C$\underline{H}_2$-N). t_R (C18 Gravity-SB, method 1): 18.2 min.

Alkyne N-oxide 15. Under nitrogen atmosphere a solution of 3-dimethylamino-1-propyne (**13**) (2.00 g, 24.0 mmol, 1.00 eq.) in anhydrous CH$_2$Cl$_2$ (24 mL) was cooled to 0 °C via an ice bath and subsequently a solution of mCPBA (75% with H$_2$O, 5.54 g, 24.0 mmol, 1.00 eq.) in anhydrous CH$_2$Cl$_2$ (24 mL) was added in a single portion. The reaction mixture was warmed to room temperature and stirred at this temperature for 3 h. Afterwards the reaction mixture was passed through a plug of alkaline alumina. The plug was first eluted with CH$_2$Cl$_2$ followed by CH$_2$Cl$_2$/MeOH 95 : 5. All volatiles were removed in vacuo (bath temperature at room temperature), the product was dried under high vacuum and 3-dimethylamino-1-propyne N-oxide **15** (1.98 g, 83%) was obtained as a colourless solid. As the product was temperature-sensitive and unstable in its solid form, it was immediately dissolved in MilliQ H$_2$O to yield a stable 3 M aq. stock solution which was stored at 4 °C. HRMS (ESI) m/z [M+H]$^+$ calcd for C$_5$H$_{10}$NO$^+$: 100.0757, found: 100.0761. ^{1}H-NMR (D$_2$O, 300 MHz) δ = 4.20 (s, 2H, C$\underline{H}_2$), 3.35 (s, 1H, C≡C$\underline{H}$), 3.30 (s, 6H, C$\underline{H}_3$).

Bn$_3$-NOx$_3$-PCTA 10. Under nitrogen atmosphere a mixture of DMF/H$_2$O (7 : 1, 1.80 mL) was degassed by purging the solution with nitrogen gas for 15 min under vigorous stirring. Afterwards CuI (8.90 mg, 47.0 μmol, 0.10 eq.) and sodium ascorbate (18.5 mg, 93.0 μmol, 0.20 eq.) were added and the degassing process was allowed to proceed for further 5 min. Following (R,R,R)-Bn$_3$-PCTAZA **8** (0.40 g, 0.47 mmol, 1.00 eq.) as a solution in DMF (0.25 mL) and an aq. solution of 3-dimethylamino-1-propyne N-oxide (**15**) (3 M in H$_2$O, 2.8 mL, 8.39 mmol, 18.0 eq.) were both added in one portion. The reaction mixture was warmed to 55 °C and stirred at this temperature for 65 min. All volatiles were removed in vacuo and the crude product was obtained as a yellowish wax. The crude product was purified via reversed phase flash chromatography (loaded as solution in

H$_2$O (2 mL), 15 μm C18AQ silica, Interchim cartridge F0012, 100% H$_2$O 5 CV, then gradient to 100% MeCN in 10 CV, 100% MeCN 5 CV. After lyophilization Bn$_3$-NOx$_3$-PCTA **10** (392 mg, 73%) was obtained as a beige lyophilisate. HRMS (ESI) m/z [M+H]$^+$ calcd for C$_{59}$H$_{78}$N$_{16}$O$_9^+$: 1154.6133, found: 1154.6100. ^{1}H-NMR (D$_2$O, 600 MHz) δ = 8.31 (1H, s, $\underline{H}_{triazole}$ sidearm opposite pyridine), 8.11 (2H, s, $\underline{H}_{triazole}$ sidearms next to pyridine), 7.95 (1H, t, $^3J_{H,H}$ = 7.81 Hz, C$_{pyridine}$-$\underline{H}$ para to N$_{pyridine}$), 7.43–7.27 (13H, m, CH$_2$-Ph-$\underline{H}$ sidearms next to pyridine, C$_{pyridine}$-$\underline{H}$ meta to N$_{pyridine}$, CH$_2$-Ph-H sidearm opposite pyridine), 7.20 (2H, dd, $^3J_{H,H}$ = 7.71 Hz, CH$_2$-Ph-$\underline{H}$), 7.02 (2H, dd, $^3J_{H,H}$ = 7.51 Hz, CH$_2$-Ph-$\underline{H}$), 5.12 (2H, m, Ph-C$\underline{H}_2$-, sidearm opposite pyridine), 5.05–4.87 (4H, m, Ph-C$\underline{H}_2$-, sidearms next to pyridine), 4.75–4.70 (2H, m, C$\underline{H}_2$-CH$_2$-triazole sidearm opposite pyridine), 4.65–4.60 (4H, m, C$\underline{H}_2$-NOx, sidearms next to pyridine), 4.56 (2H, s, C$\underline{H}_2$-NOx sidearm opposite pyridine), 4.45–4.22 (m, 4H, CH$_2$-C$\underline{H}_2$-triazole sidearms next to pyridine), 4.00–3.97 (5H, m, BnO$_2$C-C$\underline{H}$-), 3.84 (2 H, m, Pyridine-C$\underline{H}_2$), 3.45 (2H, m, Pyridine-C$\underline{H}_2$), 3.25 (12H, d, $^4J_{H,H}$ = 7.35 Hz, N(C$\underline{H}_3$)$_2$-O sidearms next to pyridine), 3.22 (6H, d, $^4J_{H,H}$ = 3.86 Hz, N(C$\underline{H}_3$)$_2$-O sidearm opposite pyridine), 2.94–2.59 (8H, m, N-C$_2\underline{H}_4$-N), 2.42–2.36 (4H, m, CH-C$\underline{H}_2$), 2.26–2.14 (2H, m, CH-C$\underline{H}_2$). ^{13}C-NMR (D$_2$O, 150 MHz) δ = 173.0 (C$_{carbonyl}$), 155.4 (quart. C$_{pyridine}$), 143.3 (C$_{pyridine}$-H para to N$_{pyridine}$), 136.8 (quart. C$_{triazole}$ sidearms opposite pyridine), 136.5 (quart. C$_{triazole}$ sidearms next to pyridine), 135.1 (quart. C$_{phenyl}$ sidearms next to pyridine), 133.7 (quart. C$_{phenyl}$ sidearm opposite pyridine), 129.2, 129.0, 128.9, 128.8, 128.7, 128.6, 128.5, 127.8, 127.5 (C$_{phenyl}$, C$_{triazole}$-H), 123.03 (C$_{pyridine}$ meta to N$_{pyridine}$), 68.6 (Ph-C$\underline{H}_2$ next to pyridine), 67.5 (BnO$_2$C-C$\underline{H}$-), 63.8 (C$\underline{H}_2$-NOx next to pyridine), 63.7 (C$\underline{H}_2$-NOx opposite pyridine), 58.2 (Ph-C$\underline{H}_2$ opposite pyridine), 56.5 (N$^+$-(C$\underline{H}_3$)$_2$-O sidearms next to pyridine), 56.4 (N$^+$-(C$\underline{H}_3$)$_2$-O sidearm opposite pyridine), 52.8 (pyridine-C$\underline{H}_2$), 52.0 (pyridine-C$\underline{H}_2$), 47.8 (CH$_2$-C$\underline{H}_2$-triazole sidearms next to pyridine), 47.5 (CH$_2$-C$\underline{H}_2$-triazole sidearms opposite pyridine), 42.28 (C$\underline{H}_2$-CH$_2$-triazole), 29.4 (N-C$_2\underline{H}_4$-N), 24.1 (N-C$_2\underline{H}_4$-N). t_R (C18 Gravity-SB, method 1): 11.7 min.

Bn$_3$-SB$_3$-PCTA 9. Under nitrogen atmosphere DMF/H$_2$O 7 : 1 (8 mL) was degassed by purging the solution with nitrogen gas for 15 min under vigorous stirring. Afterwards CuI (8.90 mg, 47.0 μmol, 0.10 eq.) and sodium ascorbate (18.5 mg, 93.0 μmol, 0.20 eq.) were added and the degassing process was allowed to proceed for further 5 min. Following (R,R,R)-Bn$_3$-PCTAZA **8** (400 mg, 466 μmol, 1.00 eq.) as a solution in DMF (1.5 mL) and sulfobetaine alkyne **14** (316 mg, 1.64 mmol, 3.30 eq.) were both added in one portion. The reaction mixture was warmed to 50 °C and stirred at this temperature for 41 h during which the reaction solution became dark brown. All volatiles were removed in vacuo and the crude product was obtained as a brownish waxy solid. The crude product was purified via reversed phase flash chromatography (loaded as solution in H$_2$O (2 mL), 15 μm C18AQ silica, Interchim cartridge F0012, 100% H$_2$O 5 CV, gradient to 100% MeCN in 10 CV, 100% MeCN 5 CV. After lyophilization Bn$_3$-SB$_3$-PCTA **9** (365 mg, 53%) was obtained as colourless lyophilisate. HRMS (ESI) m/z [M+2H]$^{2+}$ calcd for C$_{68}$H$_{98}$N$_{16}$O$_{15}$S$_3^{2+}$: 737.3275, found: 737.3293. ^{1}H-NMR (D$_2$O, 600 MHz) δ = 8.45, 8.43 (s, 2H, $\underline{H}_{triazole}$ sidearms

next to pyridine), 8.26 (s, 1H, $\underline{H}_{triazole}$ sidearm opposite pyridine), 7.97–7.94 (m, 1H, $C_{pyridine}$-$\underline{H}$ *para* to $N_{pyridine}$), 7.42–7.02 (m, 17H, CH_2-Ph-$\underline{H}$, $C_{pyridine}$-$\underline{H}$ *meta* to $N_{pyridine}$), 5.11–4.86 (m, 6H, Ph-C$\underline{H}_2$), 4.70–4.31 (m, 13H, $N^+(CH_3)_2$-$\underline{CH}_2$-triazole, Pyridine-C$\underline{H}_2$, BnO_2C-C$\underline{H}$), 4.00–3.40 (m, 8H, N-C$\underline{H}_2$-C$\underline{H}_2$-N), 3.37–3.27 (m, 6H, $N^+(CH_3)_2$-$\underline{CH}_2$-CH_2), 3.09–3.02 (m, 18H, N-($\underline{CH}_3$)$_2$-O), 2.98–2.60 (m, 12H, CH_2-C$\underline{H}_2$-SO_3, CH-C$\underline{H}_2$), 2.49–2.20 (m, 12H, CH_2-C$\underline{H}_2$-SO_3, CH-C$\underline{H}_2$). ^{13}C-NMR ($CDCl_3$, 150 MHz) δ = 172.8 ($C_{carbonyl}$), 170.9 ($C_{triazole}$-H), 155.6 (HMBC, quart. $\underline{C}_{pyridine}$), 143.1 (HSQC, $C_{pyridine}$-H$_{para}$ to $N_{pyridine}$), 135.4, 135.2, 135.1 (quart. $\underline{C}_{triazole}$ and quart. C_{phenyl}), 129.3, 129.0, 128.9, 128.8, 128.7, 128.6, 128.5, 128.4, 128.2, 127.5 (C_{phenyl}-H and $C_{pyridine}$-H), 123.1 (C_{phenyl}-H), 120.8 (HSQC, C_{phenyl}-H), 68.4 (Ph-$\underline{C}H_2$), 67.5 (BnO_2C-$\underline{C}H$-), 67.3 (triazole-$\underline{C}H_2$-$N^+(CH_3)_2$), 61.8 (pyridine-$\underline{C}H_2$), 57.7, 57.6 ($N^+(CH_3)_2$-$\underline{C}H_2$-CH_2), 50.4, 50.3, 50.2 (N-($\underline{C}H_3$)$_2$-O), 47.8, 47.7, 47.2 (CH_2-$\underline{C}H_2$-SO_3, N-CH_2-$\underline{C}H_2$-triazole), 32.7, 29.7, 29.4 (HSQC, N-$\underline{C}_2H_4$-N, N-CH_2-$\underline{C}H_2$-triazole), 18.3, 18.2 ($\underline{C}H_2$-CH_2-SO_3). t_R (C18 Gravity-SB, method 1): 13.2 min.

Gd-NOx$_3$-PCTA 12a. At room temperature Bn$_3$-NOx$_3$-PCTA **10** (250 mg, 216 μmol, 1.00 eq.) was dissolved in H_2O (5 mL) and following a solution of NaOH (104 mg, 2.60 mmol, 12.0 eq.) in H_2O (1 mL) was added dropwise. The yellowish solution was stirred at room temperature for 23 h before Dowex® 50 W X8 hydrogen form, 100–200 mesh (500 mg) was added and the suspension was stirred until the pH was found to be neutral. The resin was removed *via* filtration, washed with H_2O (5 mL) and all volatiles were removed *in vacuo*. The residue was taken up in a solution of GdCl$_3$ hexahydrate (84.4 mg, 227 μmol, 1.05 eq.) in 1 M aq. NH$_4$OAc buffer (11 mL, pH 5.5) and the reaction mixture was stirred at room temperature for 3 h. Afterwards all volatiles were removed *in vacuo* (bath temperature: 55 °C) and the crude product was obtained as a yellowish oily residue. The crude product was purified *via* reversed phase flash chromatography (loaded as solution in H_2O (1.5 mL), 15 μm C18AQ silica, Interchim cartridge F0012, 3 CV 100% H_2O, then gradient to 100% MeCN in 10 CV, then 100% MeCN holding for 3 CV). After lyophilization Gd-NOx$_3$-PCTA **12a** (172 mg, 77%) was obtained as a colourless lyophilisate. HRMS (ESI) m/z [M+2H]$^{2+}$ calcd for $C_{38}H_{58}GdN_{16}O_9^{2+}$: 520.1902, found: 520.1951. t_R (C18 Gravity-SB, method 1): 2.3 min.

Gd-SB$_3$-PCTA 11a. Bn$_3$-SB$_3$-PCTA **9** (250 mg, 170 μmol, 1.00 eq.) was dissolved in THF (1 mL) and a solution of NaOH (81.4 mg, 2.04 mmol, 12.0 eq.) in H_2O (5 mL) was added dropwise. The yellowish solution was stirred at room temperature for 23 h before Dowex 50 W X8 hydrogen form, mesh 100–200 (350 mg) was added and the suspension was stirred until the pH was found to be neutral. The resin was removed *via* filtration, washed with THF/H_2O 1 : 5 (5 mL) and all volatiles were removed *in vacuo*. The residue was taken up in a solution of GdCl$_3$ hexahydrate (66.2 mg, 178 μmol, 1.05 eq.) in 1 M aq. NH$_4$OAc buffer (11 mL, pH 5.5) and the reaction mixture was stirred at room temperature for 1.5 h. All volatiles were removed *in vacuo* (bath temperature: 55 °C) and the crude product was obtained as a yellowish solid. The crude product was purified *via* reversed phase flash chromatography (loaded

as solution in H_2O (1 mL), 15 μm C18AQ silica, Interchim cartridge F0012, 3 CV 100% H_2O, then gradient to 100% MeCN in 10 CV, then 100% MeCN holding for 3 CV. After lyophilization Gd-SB$_3$-PCTA **11a** (195 mg, 85%) was obtained as a colourless lyophilisate. HRMS (ESI) m/z [M+H+Na]$^{2+}$ calcd for $C_{47}H_{76}GdN_{16}NaO_{15}S_3^{2+}$: 690.6983, found: 690.6971. t_R (C18 Gravity-SB, method 1): 9.2 min.

Eu-NOx$_3$-PCTA 12b. Bn$_3$-SB$_3$-PCTA **9** (14 mg, 12.0 μmol, 1.00 eq.) was dissolved in H_2O (1 mL) and a solution of NaOH (5.8 mg, 145 μmol, 12.0 eq.) in H_2O (0.5 mL) was added dropwise. The yellowish solution was stirred at room temperature for 17 h before Dowex 50W X8 hydrogen form, mesh 100–200 (80 mg) was added and the suspension was stirred until the pH was found to be neutral. The resin was removed *via* filtration, washed with H_2O (3 mL) and all volatiles were removed *in vacuo*. The residue was taken up in a solution of EuCl$_3$ (3.3 mg, 13.0 μmol, 1.05 eq.) in 1 M aq. NH$_4$OAc buffer (1 mL, pH 5.5) and the reaction mixture was stirred at room temperature for 3 h. All volatiles were removed *in vacuo* (bath temperature: 55 °C) and the crude product was obtained as a yellowish solid. The crude product was purified *via* reversed phase flash chromatography (loaded as solution in H_2O (0.2 mL), 15 μm C18AQ silica, Interchim cartridge F0004, 4 CV 100% H_2O, then gradient to 100% MeCN in 10 CV, then 100% MeCN holding for 3 CV). After lyophilization Eu-NOx$_3$-PCTA **12b** (6 mg, 48%) was obtained as a colourless lyophilisate. HRMS (ESI) m/z [M+2H]$^{2+}$ calcd for $C_{38}H_{59}EuN_{16}O_9^{2+}$: 518.1926, found: 518.1952. t_R (C18 Gravity-SB, method 1): 2.0 min.

Eu-SB$_3$-PCTA 11b. Bn$_3$-SB$_3$-PCTA **9** (19.5 mg, 13.0 μmol, 1.00 eq.) was dissolved in H_2O (1 mL) and a solution of NaOH (6.4 mg, 159 μmol, 12.0 eq.) in H_2O (0.5 mL) was added dropwise. The yellowish solution was stirred at room temperature for 18 h before Dowex® 50W X8 hydrogen form, mesh 100–200 (80 mg) was added and the suspension was stirred until the pH was found to be neutral. The resin was removed *via* filtration, washed with H_2O (3 mL) and all volatiles were removed *in vacuo*. The residue was taken up in a solution of EuCl$_3$ (3.6 mg, 14.0 μmol, 1.05 eq.) in 1 M aq. NH$_4$OAc buffer (1 mL, pH 5.5) and the reaction mixture was stirred at room temperature for 3.5 h. All volatiles were removed *in vacuo* (bath temperature: 55 °C) and the crude product was obtained as a yellowish solid. The crude product was purified *via* reversed phase flash chromatography (loaded as solution in H_2O (0.2 mL), 15 μm C18AQ silica, Interchim cartridge F0004, 4 CV 100% H_2O, then gradient to 100% MeCN in 10 CV, then 100% MeCN holding for 3 CV). After lyophilization Eu-SB$_3$-PCTA **11b** (10 mg, 56%) was obtained as a colourless lyophilisate. HRMS (ESI) m/z [M+2H]$^{2+}$ calcd for $C_{47}H_{77}EuN_{16}O_{15}S_3^{2+}$: 677.2059, found: 677.2052. t_R (C18 Gravity-SB, method 1): 9.3 min.

Author contributions

Conceptualization: JVF, WM; methodology, investigation, data curation: LFVS, VRS, MGK, DL, MO, DLJT; formal analysis:

LFVS, MGK, MO; project administration, resources: JVF, WM; writing – original draft: LFVS, WM; writing – review & editing: all authors; project administration: JVF, WM; supervision: NFT, MF, WM.

Conflicts of interest

JVF is a cofounder and CEO of Curadel Pharma. JVF and WM have filed a patent application on zwitterionic chelators (WO 2025059025 (A1) 2025-03-20).

Data availability

The data supporting this article have been included as part of the supplementary information (SI). Supplementary information is available. See DOI: https://doi.org/10.1039/d5tb02336j. This material contains NMR spectra and LC/MS data for new compounds and luminescence measurements of Eu-complexes.

Acknowledgements

References

1 J. Wahsner, E. M. Gale, A. Rodriguez-Rodriguez and P. Caravan, *Chem. Rev.*, 2019, **119**, 957–1057.

2 P. Marckmann, L. Skov, K. Rossen, A. Dupont, M. B. Damholt, J. G. Heaf and H. S. Thomsen, *J. Am. Soc. Nephrol.*, 2006, **17**, 2359–2362.

3 A. K. Abu-Alfa, *Adv. Chronic Kidney D.*, 2011, **18**, 188–198.

4 T. Kanda, K. Ishii, H. Kawaguchi, K. Kitajima and D. Takenaka, *Radiology*, 2014, **270**, 834–841.

5 T. Kanda, T. Fukusato, M. Matsuda, K. Toyoda, H. Oba, J. Kotoku, T. Haruyama, K. Kitajima and S. Furui, *Radiology*, 2015, **276**, 228–232.

6 R. J. McDonald, J. S. McDonald, D. F. Kallmes, M. E. Jentoft, D. L. Murray, K. R. Thielen, E. E. Williamson and L. J. Eckel, *Radiology*, 2015, **275**, 772–782.

7 D. R. Roberts, S. M. Lindhorst, C. T. Welsh, K. R. Maravilla, M. N. Herring, K. A. Braun, B. H. Thiers and W. C. Davis, *Invest. Radiol.*, 2016, **51**, 280–289.

8 M. Ramalho, J. Ramalho, L. M. Burke and R. C. Semelka, *Adv. Chronic Kidney D.*, 2017, **24**, 138–146.

9 A. Cunningham, M. Kirk, E. Hong, J. Yang, T. Howard, A. Brearley, A. Sáenz-Trevizo, J. Krawchuck, J. Watt, I. Henderson, K. Dokladny, J. DeAguero, G. P. Escobar and B. Wagner, *Front. Toxicol.*, 2024, **6**, 1376587.

10 I. A. Dekkers, R. Roos and A. J. van der Molen, *Eur. Radiol.*, 2018, **28**, 1579–1584.

11 M. Le Fur, B. F. Moon, I. Y. Zhou, S. Zygmont, A. Boice, N. J. Rotile, I. Ay, P. Pantazopoulos, A. S. Feldman, I. A. Rosales, I. How, D. Izquierdo-Garcia, L. P. Hariri, A. V. Astashkin, B. P. Jackson and P. Caravan, *Radiology*, 2023, **309**, e230984.

12 S. K. I. Funke, C. Factor, M. Rasschaert, L. Lezius, M. Sperling, U. Karst and P. Robert, *Radiology*, 2022, **305**, 179–189.

13 T. Nemeth, N. Yoshizawa-Sugata, A. Pallier, Y. Tajima, Y. Ma, E. Toth, H. Masai and Y. Yamakoshi, *Chem. Biomed. Imaging*, 2023, **1**, 157–167.

14 A. Vaidya, A. Shankardass, M. Buford, R. Hall, P. Qiao, H. Wang, S. Gao, J. Huang, M. F. Tweedle and Z. R. Lu, *Chem. Biomed. Imaging*, 2024, **2**, 560–568.

15 C. Kuhl, T. Csoszi, W. Piskorski, T. Miszalski, J. M. Lee and P. M. Otto, *Radiology*, 2023, **308**, e222612.

16 C. Robic, M. Port, O. Rousseaux, S. Louguet, N. Fretellier, S. Catoen, C. Factor, S. Le Greneur, C. Medina, P. Bourrinet, I. Raynal, J. M. Idee and C. Corot, *Invest. Radiol.*, 2019, **54**, 475–484.

17 C. Gendron, P. Bourrinet, A. Dencausse and N. Fretellier, *Invest. Radiol.*, 2024, **59**, 108–123.

18 L. A. Loevner, B. Kolumban, G. Hutóczki, K. Dziadziuszko, D. Bereczki, A. Bago and A. Pichiecchio, *Invest. Radiol.*, 2023, **58**, 307–313.

19 R. Napolitano, N. Guidolin, M. Boccalon, A. Fringuello Mingo, S. Colombo Serra, F. Buonsanti, R. Fretta, N. Demitri, A. Benyei, M. Botta, G. B. Giovenzana, F. Tedoldi and Z. Baranyai, *Adv. Sci.*, 2025, **12**, e2415321.

20 M. Holzapfel, T. Baldau, S. Kerpa, G. Guadalupi, B. Qi, Y. Liu, W. J. Parak and W. Maison, *Eur. J. Inorg. Chem.*, 2022, e202200432, DOI: 10.1002/ejic.202200432.

21 S. Kerpa, V. R. Schulze, M. Holzapfel, L. Cvancar, M. Fischer and W. Maison, *ChemistryOpen*, 2024, **13**, e202300298.

22 M. Woods, S. Aime, M. Botta, J. A. K. Howard, J. M. Moloney, M. Navet, D. Parker, M. Port and O. Rousseaux, *J. Am. Chem. Soc.*, 2000, **122**, 9781–9792.

23 H. S. Choi, K. Nasr, S. Alyabyev, D. Feith, J. H. Lee, S. H. Kim, Y. Ashitate, H. Hyun, G. Patonay, L. Strekowski, M. Henary and J. V. Frangioni, *Angew. Chem., Int. Ed.*, 2011, **50**, 6258–6263.

24 H. S. Choi, S. L. Gibbs, J. H. Lee, S. H. Kim, Y. Ashitate, F. Liu, H. Hyun, G. Park, Y. Xie, S. Bae, M. Henary and J. V. Frangioni, *Nat. Biotechnol.*, 2013, **31**, 148–153.

25 E. Kriemen, E. Ruf, U. Behrens and W. Maison, *Chem. – Asian J.*, 2014, **9**, 2197–2204.

26 S. E. Denmark and S. M. Yang, *J. Am. Chem. Soc.*, 2004, **126**, 12432–12440.

27 E. Kriemen, M. Holzapfel, E. Ruf, J. Rehbein and W. Maison, *Eur. J. Inorg. Chem.*, 2015, 5368–5378, DOI: 10.1002/ejic.201500789.

28 S. K. Singh, M. Srinivasa Reddy, M. Mangle and K. Ravi Ganesh, *Tetrahedron*, 2007, **63**, 126–130.

29 A. Beeby, I. M. Clarkson, R. S. Dickins, S. Faulkner, D. Parker, L. Royle, A. S. de Sousa, J. A. G. Williams and M. Woods, *J. Chem. Soc., Perkin Trans. 2*, 1999, 493–503, DOI: 10.1039/a808692c.

30 A. Barge, G. Cravotto, E. Gianolio and F. Fedeli, *Contrast Media Mol. Imaging*, 2006, **1**, 184–188.

31 E. Hvattum, P. T. Normann, G. C. Jamieson, J. J. Lai and T. Skotland, *J. Pharm. Biomed. Anal.*, 1995, **13**, 927–932.

32 S. Laurent, L. Vander Elst, C. Henoumont and R. N. Muller, *Contrast Media Mol. Imaging*, 2010, **5**, 305–308.

33 C. Robic, S. Catoen, M.-C. D. Goltstein, J.-M. Idée and M. Port, *Biometals*, 2011, **24**, 759–768.

34 J. M. Idée, M. Port, C. Robic, C. Medina, M. Sabatou and C. Corot, *J. Magn. Reson. Imaging*, 2009, **30**, 1249–1258.

35 J. C. Pierrard, J. Rimbault, M. Aplincourt, S. Le GreneurB and M. Port, *Contrast Media Mol. Imaging*, 2008, **3**, 243–252.

36 M. Kobus, T. Friedrich, E. Zorn, N. Burmeister and W. Maison, *J. Med. Chem.*, 2024, **67**, 5168–5184.

37 P. Caravan, J. J. Ellison, T. J. McMurry and R. B. Lauffer, *Chem. Rev.*, 1999, **99**, 2293–2352.

38 V. Jacques, S. Dumas, W. C. Sun, J. S. Troughton, M. T. Greenfield and P. Caravan, *Invest. Radiol.*, 2010, **45**, 613–624.

39 L. M. De Leon-Rodriguez, A. F. Martins, M. C. Pinho, N. M. Rofsky and A. D. Sherry, *J. Magn. Reson. Imaging*, 2015, **42**, 545–565.

40 H. W. Roesky and M. Andruh, *Coord. Chem. Rev.*, 2003, **236**, 91–119.

41 R. M. Supkowski and W. D. Horrocks, *Inorg. Chim. Acta*, 2002, **340**, 44–48.

42 E. Di Gregorio, R. Iani, G. Ferrauto, R. Nuzzi, S. Aime and E. Gianolio, *J. Trace Elem. Med. Biol.*, 2018, **48**, 239–245.

43 J. Lohrke, M. Berger, T. Frenzel, C. S. Hilger, G. Jost, O. Panknin, M. Bauser, W. Ebert and H. Pietsch, *Invest. Radiol.*, 2022, **57**, 629–638.

44 S.-L. Niu, G. Ulrich, P. Retailleau, J. Harrowfield and R. Ziessel, *Tetrahedron Lett.*, 2009, **50**, 3840–3844.

45 A. Galan, G. Gil-Ramirez and P. Ballester, *Org. Lett.*, 2013, **15**, 4976–4979.